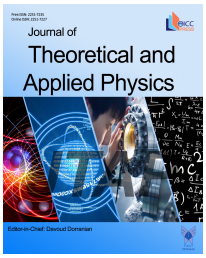

Volume 19, Issue 5, 192551 (1-11)

Journal of Theoretical and Applied Physics (JTAP)

https://doi.org/10.57647/j.jtap.2025.1905.51

Comparative structural and superconducting characterization of nanostructured $Y_3Ba_4Cu_7O_{16-\delta}$ (Y347) and $Y_3Ba_5Cu_8O_{18-\delta}$ (Y358) superconductors

Maryam Badeaa Abood[1,2,*], Emad K. Al-Shakarchi[3]

[1]*Department of Physics, College of Science, Al-Nahrain University, Baghdad, Iraq.*
[2]*Department of Physics, College of Science, University of Baghdad, Baghdad, Iraq.*
[3]*Department of Medical Physics, Dijlah University College, Baghdad, Iraq.*

[*]**Corresponding author:** maryam.b@sc.uobaghdad.edu.iq

Original Research

Received:
28 July 2025
Revised:
24 August 2025
Accepted:
9 September 2025
Published online:
31 October 2025

Abstract:

This study presents a comparative investigation of two nanostructured superconducting compounds, $Y_3Ba_4Cu_7O_{16-\delta}$ (Y347) and $Y_3Ba_5Cu_8O_{18-\delta}$ (Y358), synthesized via a modified sol-gel auto-combustion technique using metal nitrates as precursors. The synthesis process involved gelation, controlled drying, calcination, and sintering steps, which enabled the formation of single-phase orthorhombic structures, as confirmed by X-ray diffraction (XRD). The calculated lattice parameters for Y347 were a = 7.42 Å, b = 3.12 Å, and c = 19.213 Å, while Y358 exhibited values of a = 3.875 Å, b = 3.884 Å, and c = 31.03 Å. Transmission electron microscopy (TEM) revealed an average particle size of 63.36 nm for Y347 with nearly spherical morphology, whereas Y358 particles appeared as well-defined nanorods with an average diameter of 33.28 nm. Electrical resistivity (ρ–T) measurements demonstrated superconducting transition temperatures of 145 K for Y347 and 150 K for Y358, indicating enhanced superconducting performance of Y358, as evidenced by a higher Tc and well-defined nanorods morphology, likely contributing to improved interlayer coupling and charge transport. To our knowledge, this study is among the first to provide a systematic nanoscale comparison of Y347 and Y358, highlighting the influence of particle size and morphology on Tc. These results emphasize the critical influence of nanoscale morphology, lattice configuration, and preparation route on the superconducting behavior of extended Y-based cuprate phases. The findings contribute to the ongoing development of High-Tc materials with improved structural and functional properties.

Keywords: YBCO superconductors; Sol-gel auto-combustion; Y347; Y358; Superconducting transition temperature (Tc); XRD analysis; TEM analysis

1. Introduction

The discovery of high-temperature superconductivity in La-based cuprates [1] opened the door to many other copper-oxide materials. One of the most studied families is YBCO, which is made of yttrium, barium, and copper oxides. These materials are known for having zero resistance and strong magnetic properties [2]. These kinds of materials don't need extremely low temperatures like the older superconductors. These materials do not require cooling with liquid helium, which is expensive and not easy to manage. Instead, they can be cooled using liquid nitrogen [3], which makes them more suitable for practical applications. Within the YBCO family, one of the most studied compounds is $YBa_2Cu_3O_{7-\delta}$ (Y123). It shows a critical temperature close to 93 K and has an orthorhombic crystal structure that has been examined in many research works [4, 5]. The way this compound behaves as a superconductor is linked to its structure. It contains layers made of CuO_2 planes along with CuO chains [6]. Some researchers have worked on adjusting how many of these layers exist in the structure, hoping to improve its performance. One example that came from this approach is $Y_3Ba_5Cu_8O_{18-\delta}$ (Y358), which includes five CuO_2 planes and three CuO chains. This compound has reached higher critical temperatures, in some studies even above 100 K [7, 8]. There is not much research done yet on the $Y_3Ba_4Cu_7O_{16-\delta}$ (Y347) compound. It has more Cu–O layers than Y123, but fewer than Y358, so it sits somewhere between them in structure. For this reason, it is thought that

Y347 may have interesting properties, but more study is still needed to confirm that [9]. Previous research on YBCO superconductors has mainly focused on the Y123 and Y358 phases, where structural optimization and oxygenation effects were studied extensively. However, no work has yet reported the successful synthesis of the Y347 phase. This absence of information represents a clear research gap in the field. The novelty of the present work lies in the preparation of the Y347 phase for the first time, as a new member of the YBCO family, and in its direct comparison with the Y358 phase to reveal the influence of nanostructure and morphology on the superconducting transition temperature. In this study, Y347 and Y358 were both prepared using the sol-gel method along with auto-combustion. This preparation route was selected because it can produce small, evenly distributed particles. The samples were examined using XRD for structural analysis, TEM for observing particle size and shape, and resistivity measurements to find the critical temperature. This study is designed to:

- Exploration of structural, morphological, vibrational, and superconducting characteristics of $Y_3Ba_4Cu_7O_{16-\delta}$ (Y347) and $Y_3Ba_5Cu_8O_{18-\delta}$ (Y358).
- Evaluation based on XRD, FTIR, TEM, and resistivity measurements to assess material properties.
- Assessment of practical potential of both compounds for high-performance superconducting systems.
- First-time investigation of nanostructured Y347, providing a novel comparison with Y358 and highlighting the effect of particle size and morphology on Tc.

2. Experimental

In this study, Y-347 and Y-358 superconducting samples were prepared by using the sol-gel technique along with auto-combustion. This approach was chosen because it can give small and evenly distributed particles. For the starting materials, yttrium, barium, and copper nitrates were used: $Y(NO_3)_3 \cdot 6H_2O$, $Ba(NO_3)_2$, and $Cu(NO_3)_2 \cdot 3H_2O$. The amounts were measured based on the atomic ratios: 3 parts Y, 4 parts Ba, and 7 parts Cu for Y-347; and 3:5:8 for Y-358 Citric acid monohydrate was used along with them as the fuel. Each compound was first dissolved on its own in about 10 mL of distilled water, while stirring with a magnetic stirrer. Once the solutions were mixed, the solution turned turquoise, indicating the formation of a homogeneous metal–citric acid complex. To adjust the pH, ammonium hydroxide was added drop by drop until it reached 7. The mixture was then placed on a hot plate and heated to around 80 °C to help it turn into a gel. Later, the temperature was raised again—this time above 180 °C to start the combustion reaction; At this point, a self-sustained combustion reaction occurred, as illustrated in figure 1. It lasted for about 20 to 30 seconds and gave a brown powder. The powder was dried at 250 °C for one hour to remove water. Then it was heated at 750 °C for 12 hours (with 10 °C per minute ramp) to remove leftover nitrates. If the phase was not correct after XRD test, this step was repeated.

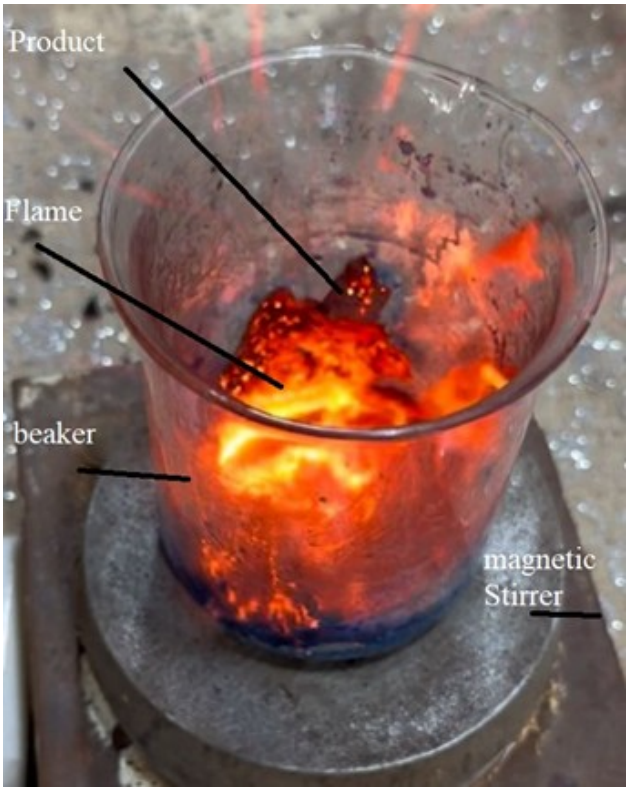

Figure 1. Illustration of the auto-combustion process.

The powder was pressed into round pellets, 12 mm wide and 4 mm thick, using pressure between 8 to 10 tons. These pellets were sintered in oxygen at 850 °C for 24 hours to complete the crystallization [10]. The electrical resistivity measurements were carried out using the standard four-probe method (figure 2). A constant current was applied through the outer probes, while the potential difference was recorded across the inner probes. The resistivity (ρ) was calculated using the relation: $\rho = \frac{R \cdot A}{L}$ where $R = V/IR, V/I$ is the measured resistance, A is the cross-sectional area of the pellet, and L is the distance between the voltage contacts. In this study, a geometrical correction factor was applied according to the actual pellet dimensions. The samples were thin pellets with a thickness of ~ 0.3 mm and diameter of ~ 0.8 cm, and silver paste was used to ensure good electrical contact between the electrodes and the sample surface. Figure 2 shows the measurement setup and sample positioning inside the cryogenic system (figure 3). All electrical measurements were performed during cooling with liquid nitrogen to determine the superconducting transition temperature Tc. To ensure reproducibility and accuracy, the measurements were repeated on six different pellets for each composition (Y-347 and Y-358). A summary of the process steps is illustrated in figure 4.

3. Result and discussion

The X-ray diffraction (XRD) pattern of $Y_3Ba_4Cu_7O_{16-\delta}$ (Y347), shown in figure 5, reveals distinct changes in crystallographic structure before and after calcination. Initially, the pattern exhibits broad and low-intensity peaks at $2\theta = 20.4°$, $23.8°$, $29.28°$, $31.5°$, $35.7°$, $45.4°$, $48.7°$,

Figure 2. Schematic diagram of the standard four-probe resistivity measurement setup.

54.23°, 60.03°, 62.8°, and 68.26°, corresponding to crystallographic planes such as (104), (200), (111), (113), (115), (311), (400), (020), (220), (0113), and (2113). These features are indicative of poor crystallinity and the presence of disordered or mixed phases, as commonly observed in early-stage YBCO-type materials [11].

After calcination, the XRD peaks become sharper and more intense, suggesting significant improvement in phase purity and crystal alignment. Some peaks appear at slightly adjusted positions (e.g., $2\theta = 22.15°$, 23.97°, and 31.42°). The narrowing of peaks reflects enhanced atomic ordering and an increase in crystallite dimensions, likely resulting from the coalescence of adjacent nanocrystals during calcination. This process reduces grain boundary area and internal defects, contributing to a more coherent and stable lattice structure. Such crystallite growth has been correlated with improved carrier mobility and reduced resistive grain boundaries in Y-based superconductors [12]. According to Table 1, the unit cell parameters decreased from a = 7.47 Å, b = 3.38 Å, c = 21.333 Å to a = 7.42 Å, b = 3.12 Å, c = 19.213 Å, confirming the structural densification post-calcination. The orthorhombicity value increased from 0.370 to 0.407, indicating enhanced directional anisotropy, which often signifies a transition toward a more thermodynamically stable phase beneficial for superconductivity [12]. The calculated crystallite size after calcination reached 75.93 nm, based on the Debye–Scherrer equation, which aligns with expected values for optimized YBCO grains [13]. For comparison, the XRD pattern of $Y_3Ba_5Cu_8O_{18-\delta}$ (Y358) in figure 6 also demonstrates structural refinement post-calcination. Before heat treatment, broad peaks at $2\theta = 23.6°$, 32.3°, 40.05°, 46.5°, 58.05°, 68.1°, and 77.3° correspond to planes (010), (108), (118), (020), (128), $(22\bar{0})$, and (308). Post-calcination, additional high-intensity reflections appear, and secondary-phase signals are suppressed, indicating a well-formed orthorhombic phase (Pmm2 symmetry) with lattice parameters a = 3.875 Å, b = 3.884 Å, and c = 31.03 Å [14]. The relatively long c-axis, approximately triple that of Y123, reflects the inclusion of additional Cu–O_2 planes-a key structural feature contributing to elevated superconducting performance [15, 16].

The orthorhombicity (0.00116) and crystallite size (38.8 nm) indicate a compact nanostructure with minimal in-plane distortion and enhanced flux pinning potential [17]. These observations demonstrate that both compounds undergo crystallographic improvement after calcination; however, Y347 exhibits larger grains and higher anisotropy, while

Figure 3. Photograph of the sample mounted inside the cryogenic measurement system.

Figure 4. Step-by-step photographic representation of the preparation procedure under the mentioned experimental conditions.

Y358 maintains finer crystallite dimensions and lower lattice distortion, consistent with their respective superconducting behaviors.

The summarized values for crystallite size, orthorhombic distortion, unit cell dimensions, and oxygen concentration of the prepared superconducting samples are listed in Table 1.

The FTIR spectrum of Y347 (figure 7) covers the range $400 - 4000\ cm^{-1}$ and reveals key features related to its chemical composition and bonding. A distinct absorption band at $1417.95\ cm^{-1}$ corresponds to carbonate groups (CO_3^{2-}), likely from residual precursors not fully decomposed during initial heat treatment, consistent with similar observations in oxide materials prepared via comparable methods [16]. Another band at $1637.66\ cm^{-1}$ is attributed to H–O–H bending vibrations, indicating adsorbed moisture

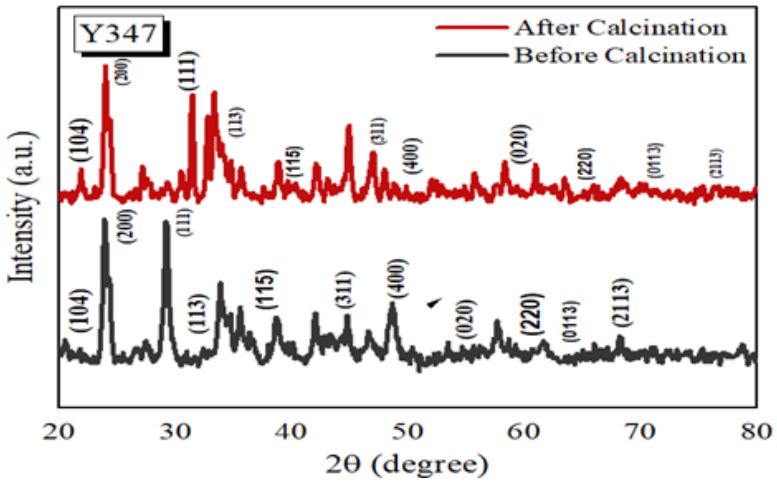

Figure 5. XRD patterns of Y347 superconductor before and after calcination.

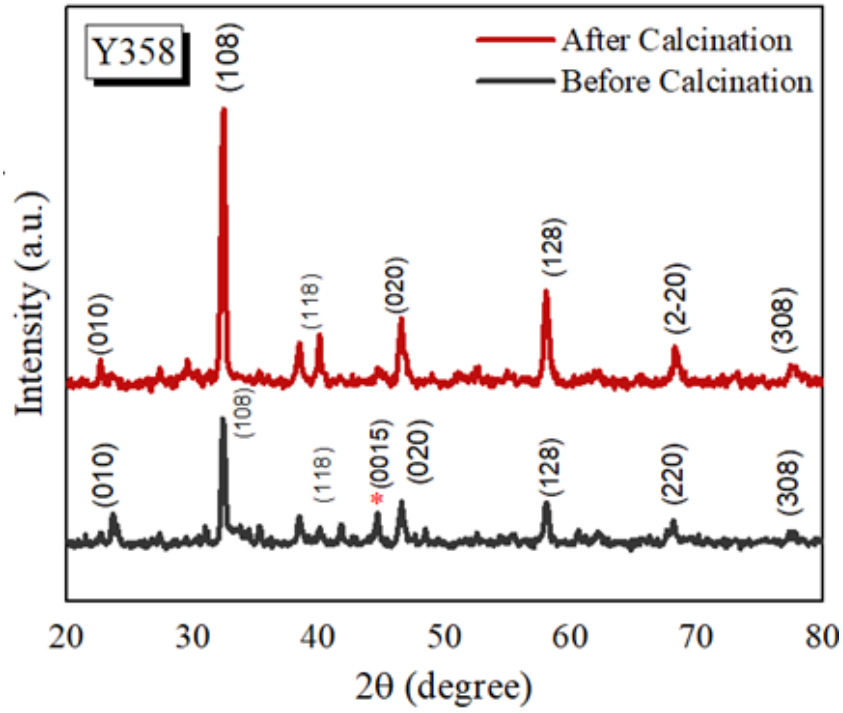

Figure 6. XRD patterns of Y358 superconductor before and after calcination.

on the powder surface, a common occurrence in ceramic superconductors stored under ambient conditions. The most significant absorption peaks appear below 700 cm^{-1}, at 692.49, 646.69, 605.69, 588.49, and 531.65 cm^{-1}. These bands correspond primarily to Cu–O and Ba–O stretching vibrations within the CuO_2 planes, a fundamental structural unit in High-Tc YBCO-type superconductors [18]. Notably, no peaks associated with nitrate groups were observed, implying effective removal of precursors and contaminants through heat treatment, supporting the formation of a clean superconducting phase. This conclusion aligns with XRD results shown in figure 3, which indicate enhanced crystallinity and phase purity in Y347. Furthermore, the assignment of FTIR peaks was supported by quantum-mechanical calculations using Schrödinger's equation, where the wavenumber is related to bond energy and bond extension. In this context, the graphical analysis (figure 6) shows that the intersection of the two curves represents the effective value of bond stretching, which is consistent with the main Cu–O absorption observed near 1059 cm^{-1}. Quantitative analysis based on FTIR data using Schrödinger's equation $E = \frac{\hbar^2 K^2}{2m}$ expressed in terms of the wave number k while all other parameters are physical constants in electron volt units) (Table 2) shows a direct correlation between increasing wavenumber and bond energy, alongside decreasing bond length. The curves for bond energy and stretching intersect near 1068 cm^{-1}, with an energy of approximately 26.6 eV and a bond length close to 6×10^{-3} cm, matching the stable bonding environment reflected by the FTIR peak at 1059 cm^{-1} (figure 8).
Similarly, the FTIR spectrum of Y358 (figure 9) exhibits features across a broad wavenumber range. Peaks at 3778 cm^{-1} and 1540 cm^{-1} indicate the presence of O–H stretching and bending vibrations, respectively, suggesting some adsorbed water likely due to sample handling or drying conditions. An absorption band at 2009 cm^{-1} corresponds to physically adsorbed CO_2 molecules (physisorption), a phenomenon observed in other YBCO-type compounds [19].
In the fingerprint region below 600 cm^{-1}, bands at 411, 450, and 495 cm^{-1} are attributed to metal–oxygen vibrations involving Y–O, Ba–O, and Cu–O bonds, confirming the structural integrity of the CuO_2 planes characteristic of YBCO superconductors [20, 21]. Calculated bond energies for these bands range between 4.02 and 5.82 eV with corresponding bond lengths from 15.26 to 12.68 $\times 10^{-3}$ cm, demonstrating strong metal–oxygen coordination essential for superconductivity. Absence of nitrate and carbonate peaks in high wavenumber regions confirms effective calcination and phase purity, consistent with the improved

Table 1. Summary of crystallite size, orthorhombic distortion, unit cell dimensions, and oxygen concentration for the prepared superconducting samples.

Superconductor	a (Å)	b (Å)	c (Å)	D (nm)	Orthorhombicity (b-a)/(b+a) [12, 14]	Oxygen content
Y347	7.42	3.12	19.213	75.934	0.407	15.9
Y358	3.875	3.884	31.03	38.848	0.00116	17.92

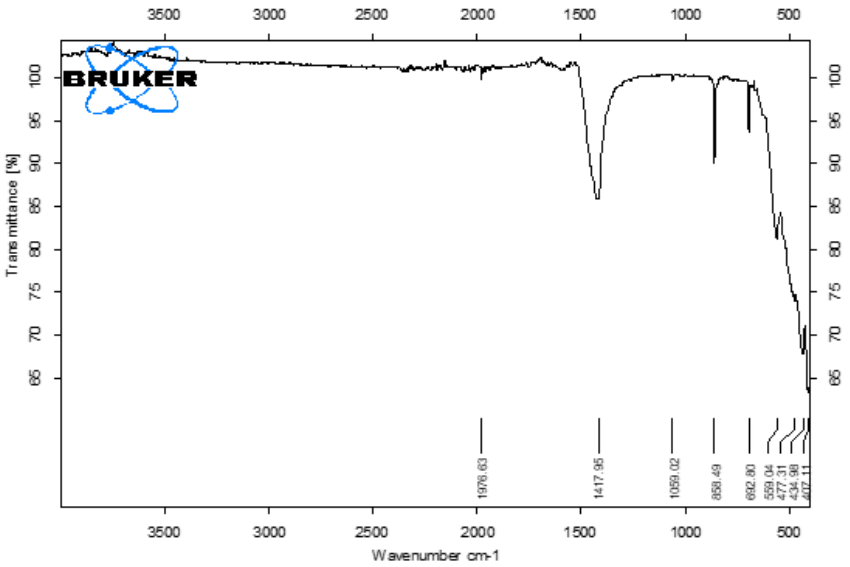

Figure 7. FTIR spectrum of the Y347 superconductor after calcination.

Table 2. The calculated bond energy and bond stretching in the Y347 and Y358 superconducting compounds.

Wave number (cm^{-1}) of Y347	Energy (eV)	Bond stretching $\times 10^{-3}$ (cm)	Wave number (cm^{-1}) of Y358	Energy (eV)	Bond stretching $\times 10^{-3}$ (cm)
407.11	3.93463	15.4336	411.72	4.0242	15.2608
434.98	4.49178	14.4448	450.99	4.8285	13.932
477.31	5.40856	13.1637	495.42	5.8267	12.6825
559.04	7.41936	11.2392	1540.66	56.35	4.0782
692.8	11.3945	9.06928	1962.2	91.4044	3.2021
858.49	17.4965	7.31889	1976.39	92.7312	3.1791
1059.02	26.6249	5.9330	2009.42	95.8566	3.1268
1417.95	47.731	4.4311	3649.64	316.2137	1.7215
1976.63	92.753	3.1787	3778.98	339.0235	1.6626

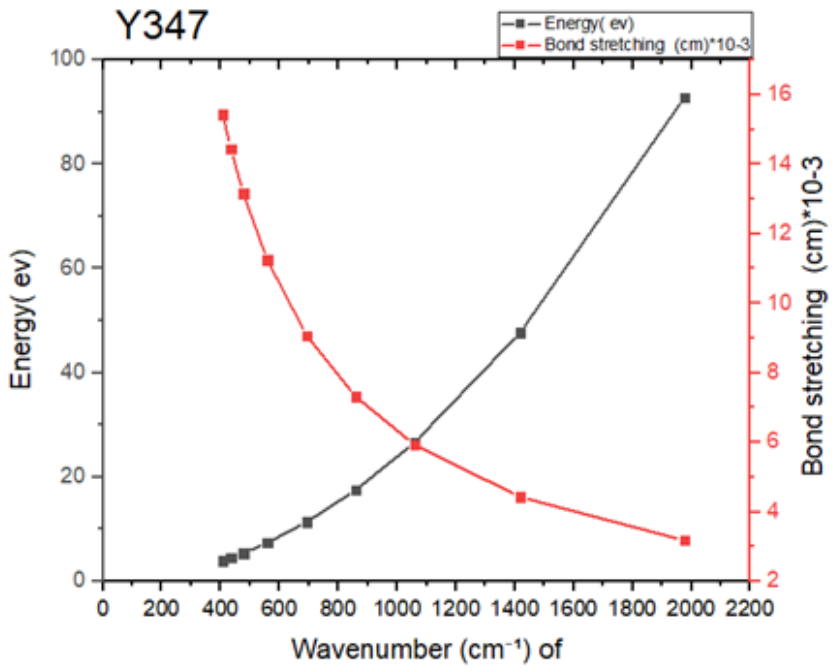

Figure 8. Indicates the behavior of bond energy and bond stretching in Y347.

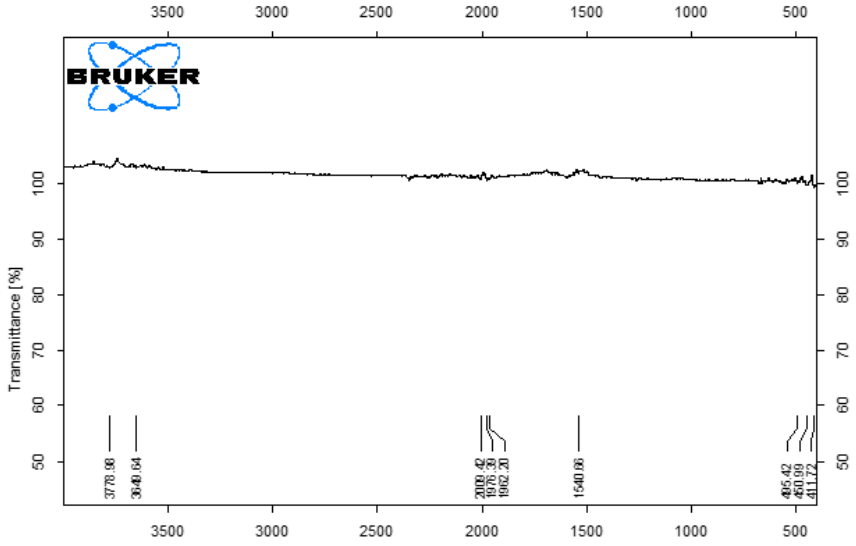

Figure 9. FTIR spectrum of Y358 superconductor.

crystal structure observed in XRD (figure 6). The trends of increasing bond energy and decreasing bond length intersect near 1800 cm^{-1} with an energy of $\sim$ 78.5 eV and bond length approximately 3.5×10^{-3} cm, as summarized in Table 2 and illustrated in figure 10.

Transmission electron microscopy (TEM) revealed distinct morphological features for the Y347 and Y358 compounds, consistent with their synthesis via the sol-gel autocombustion route. In the TEM image of Y347 (figure 11), the particles show rounded morphology with moderate dispersion and minimal agglomeration. The grain boundaries appeared mostly well-defined, indicating minimal coalescence during calcination. Particle size analysis showed a broad distribution ranging from approximately 23 nm to 134 nm, with an average grain size of 63 nm (Table 3). The average particle sizes were obtained by analyzing multiple TEM images using ImageJ software. Measurements across different regions and samples provided consistent values, supporting the reported particle sizes without requiring a histogram. This variation likely reflects a multi-stage nucleation process, which is characteristic of sol-gel-derived materials, as also noted by Pasieczna-Patkowska [20]. The presence of a few larger grains may be attributed to mild thermal merging during the heat treatment, a phenomenon frequently reported in nanostructured oxide systems [22]. These morphological findings align with the XRD results, which indicate relatively broader peaks for Y347, consistent with increased lattice strain and a wider grain size distribu-

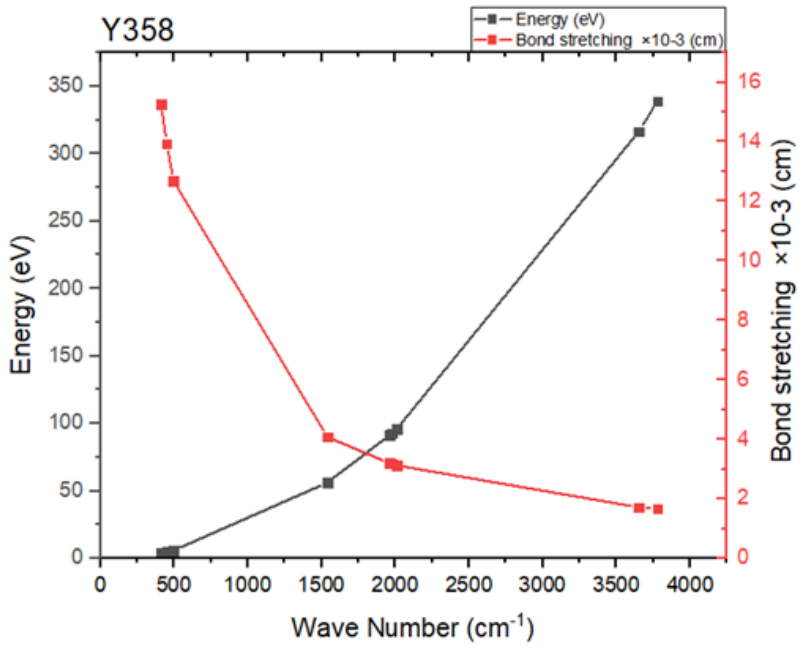

Figure 10. indicates the behavior of bond energy and bond stretching in Y358.

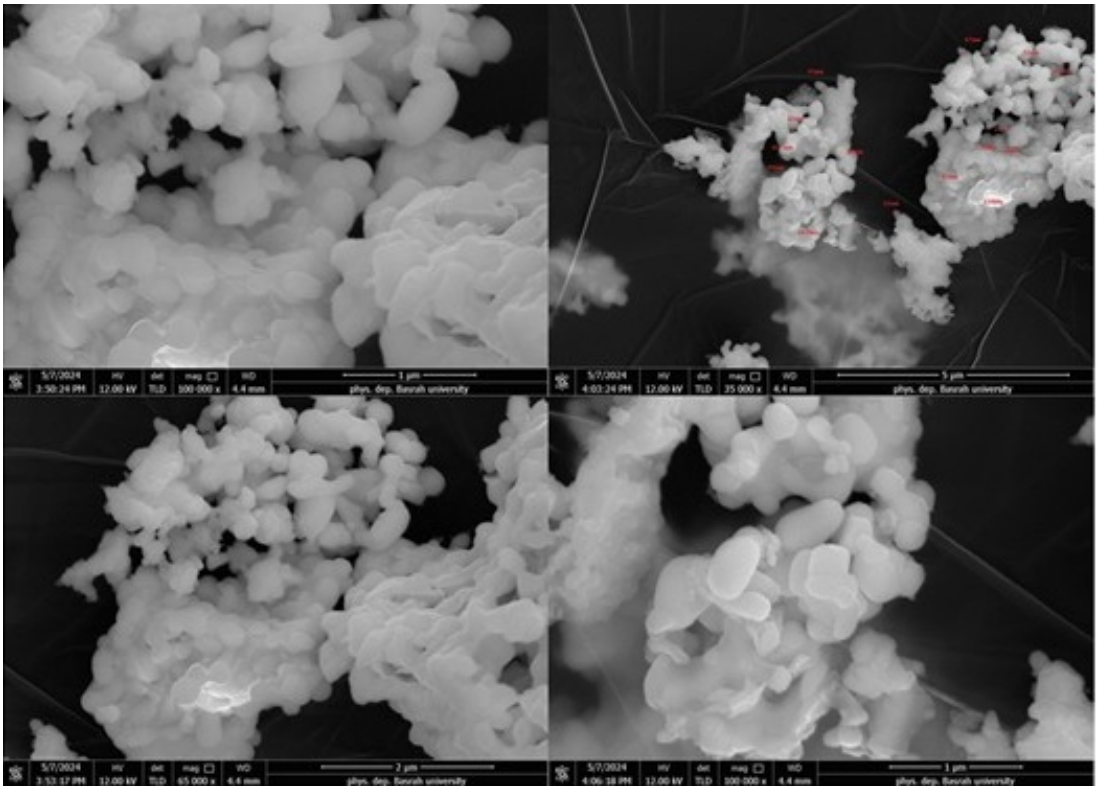

Figure 11. TEM images of Y347 superconductors recorded at different magnifications.

tion.

In contrast, the TEM image of the Y358 compound (figure 12) shows a distinctly anisotropic morphology, with particles appearing as elongated nanorods. These rod-shaped grains exhibited diameters ranging from approximately 17 nm to 54 nm, with an average diameter of 33.28 nm (Table 4). The formation of such elongated structures is indicative of directional grain growth, which may arise due to local inhomogeneities in reaction conditions, such as temperature gradients or oxygen availability [21]. In some regions, the rods appeared weakly clustered, likely due to van der Waals attractions or capillary forces during the drying phase. This moderate aggregation is typical of high-surface-area nanomaterials synthesized without stabilizing agents and has been linked to thermodynamic stabilization mechanisms [22]. Unlike the more isotropic grains of Y347, the anisotropic growth observed in Y358 may contribute to enhanced current flow directionality in the superconducting state, provided that grain connectivity remains uninterrupted. Such morphological differences between the two

Table 3. Particle size statistics of Y347 (ImageJ analysis).

Particle size of Y347 by Imagej software							
		Area	Mean	Min	Max	Angle	Length
1		38.104	187.154	164	195.867	-172.405	23.353
2		88.115	197.189	176	218.347	158.499	55.453
3		59.537	187.518	163.333	205.139	-163.74	37.745
4		130.981	179.576	98.794	210	-175.764	83.561
5		102.403	182.989	160.429	199.427	117.181	64.88
6		69.063	189.603	174.524	207.286	-149.744	43.769
7		209.57	197.021	182.904	210.841	-179.349	134.789
8	Mean	99.68186	188.7214	159.9977	206.701	-80.7603	63.36429
9	SD	52.83018	6.115139	26.09052	6.935633	138.9832	34.25849
10	Min	38.104	179.576	98.794	195.867	-179.349	23.353
11	Max	209.57	197.189	182.904	218.347	158.499	134.789

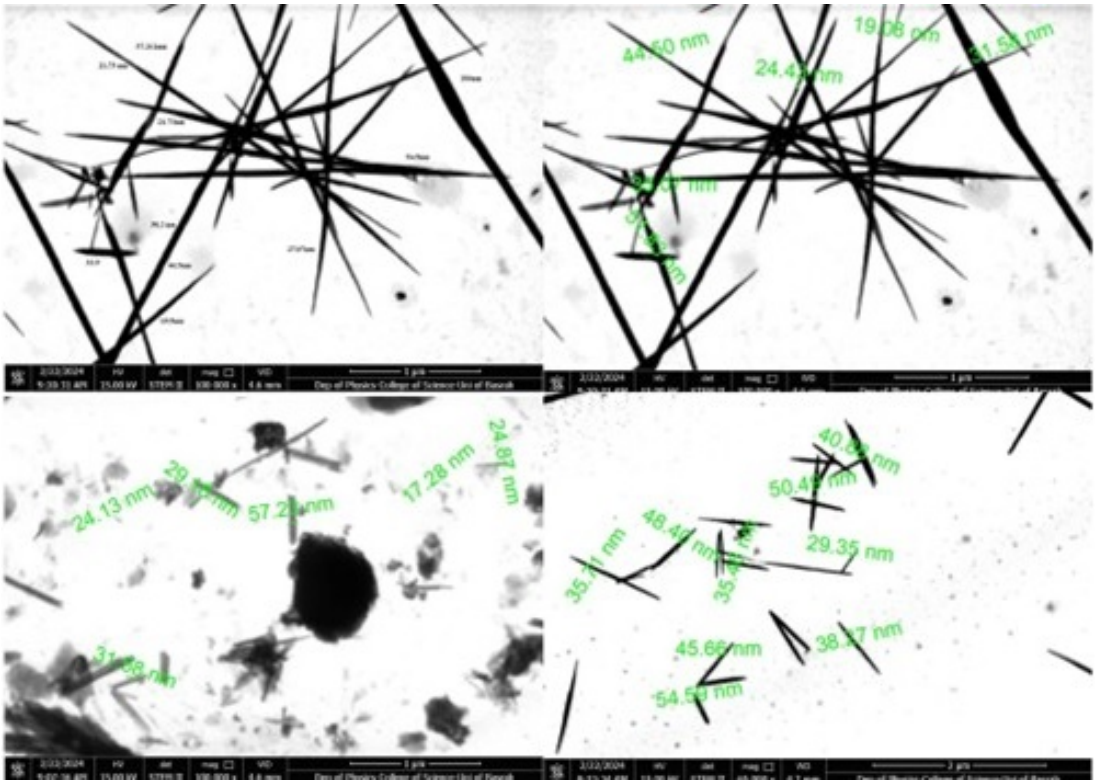

Figure 12. TEM images of Y358 recorded at different magnifications.

compounds highlight the sensitivity of microstructure to synthesis dynamics and support the structural interpretations derived from XRD analysis. To validate the TEM observations, particle sizes were measured using ImageJ software across multiple regions. For Y347, the grain diameters ranged between 23 and 134 nm with an average of $\sim$ 63 nm, whereas Y358 nanorod diameters ranged between 17 and 54 nm with an average of $\sim$ 33 nm. The statistical parameters (mean, SD, min, and max) are summarized in Table 3 and Table 4.

The resistivity behavior of the $Y_3Ba_4Cu_7O_{16-\delta}$ (Y347) superconductor is shown in figure 13. The onset of superconductivity appears at 145 K, with a complete transition to the zero-resistance state at 137 K, yielding a transition width (ΔTc) of approximately 8 K. This relatively narrow transition reflects a homogeneous superconducting phase

Table 4. Particle size statistics of Y358 (ImageJ analysis).

Particle size of Y358 by Imagej software							
		Area	Mean	Min	Max	Angle	Length
1		109.965	8021.309	0	37906.11	167.005	37.212
2		65.979	11510.74	386.833	39649.56	-129.806	21.736
3		65.979	9551.528	2271.5	33176.33	-90	21.736
5		153.951	1625.01	0	18098	-95.711	54.422
6		109.965	1131.106	0	10641	-45	38.291
7		95.303	1813.487	0	23566	-80.538	32.939
8		80.641	2552.636	0	17225	180	27.076
9		58.648	4474.658	6.857	15579.67	-56.31	19.525
10		131.958	2459.982	0	19878	-54.462	46.583
11	Mean	96.93211	4793.384	296.1322	23968.85	-22.758	33.28
12	SD	30.67318	3667.883	708.6882	9830.582	107.697	11.34734
13	Min	58.648	1131.106	0	10641	-129.806	19.525
14	Max	153.951	11510.74	2271.5	39649.56	180	54.422

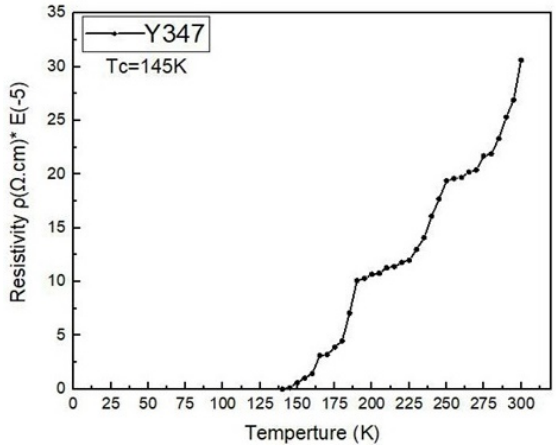

Figure 13. Resistivity curve of Y347 superconductor obtained at different temperatures.

and good structural ordering, typical of type-II superconductors. The resistivity in the normal state was measured to be about $0.8 \times 10^{-5}\Omega$·cm, corresponding to an electrical conductivity of approximately 1.25×10^{5} $(\Omega\cdot\text{cm})^{-1}$. This high conductivity indicates an adequate carrier density, likely influenced by the oxygen content per unit cell and the number of CuO_2 planes. The presence of multiple CuO_2 planes in Y347 may contribute to enhanced interlayer coupling and charge transport, which is consistent with previous studies on extended YBCO phases [23].

As for $Y_3Ba_5Cu_8O_{18-\delta}$ (Y358), the resistivity curve shown in figure 14 reveals a superconducting transition starting at approximately 150 K (midpoint of the transition, corresponding to 50% of the resistance drop) and reaching zero resistance around 140 K. The broader transition width (ΔTc $\approx$ 10 K) suggests a gradual development of the superconducting phase across the material. Above Tc, the resistivity was recorded at 0.4×10^{-5} Ω·cm, which is noticeably lower than that of Y347 and even typical Y123 compounds, indicating improved metallicity. This improvement is due to the fact that Y358 has more CuO_2 planes, which makes it easier for charges to move across the lattice. Also, the higher oxygen concentration in this compound probably

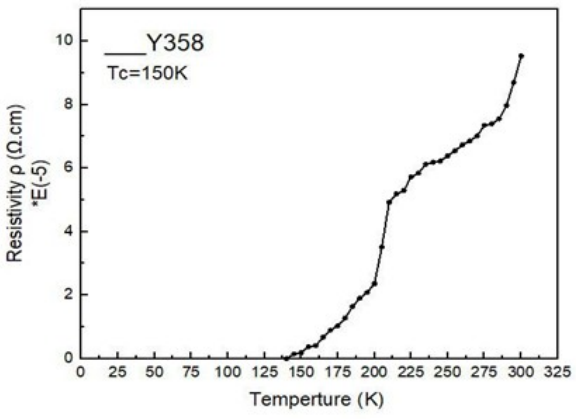

Figure 14. Resistivity curve of Y358 superconductor obtained at different temperatures.

helps the observed rise in conductivity and sharper superconducting behavior, as shown by Ghahramani et al. [15] and Shoushtari et al. [24]. The electrical results are in line with the TEM results, which showed nanorods-like features that may help with. The value of Tc was consistently confirmed by resistivity measurements conducted on more than six samples for each compound, independently tested in multiple laboratories, including the Solid State Physics Laboratory at Al-Nahrain University and the Department of Physics, College of Education for Pure Science – Ibn Al-Haytham, University of Baghdad. We should make emphasize that this result need further measurements through magnetic characterization and we are in the process of doing so.

4. Conclusion

The experimental comparison between the two synthesized superconducting compounds highlights the superior structural and functional properties of $Y_3Ba_5Cu_8O_{18-\delta}$ (Y358) relative to $Y_3Ba_4Cu_7O_{16-\delta}$ (Y347). TEM images revealed that Y358 exhibits smaller and more homogeneously distributed grains, resulting in fewer grain boundaries that may reduce electron scattering and enhance current flow. These microstructural features align with the more intense and narrower peaks observed in the XRD pattern of Y358, suggesting improved crystallinity and a finer crystallite size. FTIR analysis confirmed the presence of strong Cu–O stretching vibrations in both samples, yet the sharper absorption band in Y358 implies stronger interatomic bonding. Y358 had a greater superconducting transition temperature (Tc = 150 K) than Y347 (Tc = 145 K), and its normal-state resistivity was lower. These variables together show that Y358's better superconducting behavior is intimately linked to its finer grain structure, stable lattice framework, and strong Cu–O connections. In addition, the superior performance of Y358 may also be related to a more favorable oxygen stoichiometry (δ), which is known to strongly influence carrier concentration and Cu–O bond strength in YBCO systems. Although δ values were not directly measured in this work, the higher crystallinity observed in Y358 suggests improved oxygen ordering. Further validation by Raman or EDS analysis would strengthen this interpretation and is recommended for future studies. The superconducting transition temperature (Tc) was supported by consistent resistivity measurements performed on multiple samples across different laboratories. However, further magnetic characterization, including ZFC/FC curves and AC susceptibility, is essential to confirm the bulk nature of superconductivity and validate the observed Tc values. Given its enhanced superconducting properties, $Y_3Ba_5Cu_8O_{18-\delta}$ (Y358) may be a promising candidate for applications in high-field magnets, energy-efficient power transmission lines, and superconducting electronic devices. Future work should focus on optimizing synthesis parameters to further improve Tc and critical current density (Jc), as well as performing detailed magnetic and transport measurements under varying environmental conditions to assess long-term performance stability.

Authors Contribution
The intellectual substance, idea, and design of this study, or the analysis and interpretation of the data (if applicable), as well as the manuscript's writing, were all sufficiently contributed to by each author.

Availability of data and materials
The data that support the findings of this study are available from the corresponding author upon reasonable request.

Conflict of interests
The authors declare that they have no known competing financial interests or personal relationships that could have appeared to influence the work reported in this paper.

References

[1] Bednorz. J. G and Müller. K. A. "Possible high Tc superconductivity in the Ba-La-Cu-O system". *Z. Phys. B - Condensed Matter*, **64**: 189–193, 1986.

[2] Schneemeyer. L. F, Waszczak. J. V, Siegrist. T, van Dover. R. B, Rupp. L. W, Batlogg. B, Vava. R. J, and Murphy. D. W. "Superconductivity in $YBa_2Cu_3O_7$". *Nature*, **328**(13):601–603, 1987.

[3] Bussmann-Holder. A and Keller. H. "High-temperature superconductors: underlying physics and applications". *Z. Naturforsch. B*, **75** (1–2):3–14, 2020.

[4] Schuller. I. K, Hinks. D. G, Beno. M. A, Capone II. D. W, Soderholm. L, Locquet. J.-P, Bruneel. Y, Segre. C. U, and Zhang. K. "Structural phase transition in $YBa_2Cu_3O_{7-\delta}$: the role of dimensionality for high temperature superconductivity". *Solid State Commun.*, **63**(5): 385–388, 1987.

[5] Holland. G. F and Stacy. A. M. "Physical properties of the quaternary yttrium barium copper oxide superconductor $YBa_2Cu_3O_{7-\delta}$". *Acc. Chem. Res.*, **21**(1):8–15, 1988.

[6] Harabor. A, Rotaru. P, Harabor. N. A, Nozar. P, and Rotaru. A. "Orthorhombic YBCO-123 ceramic oxide superconductor: Structural, resistive and thermal properties". *Ceramics International*, **45**(2): 2899–2907, 2019.

[7] Khosroabadi. H, Rasti. M, and Akhavan. M. "Structural analysis of $Y_3Ba_5Cu_8O_{19-\delta}$ high-Tc superconductor by ab initio density functional theory". *Physica C: Superconductivity and Its Applications*, **497**:84–88, 2014.

[8] Aliabadia. A, Farshchib. Y. A, and Akhavan. M. "A new Y-based HTSC with Tc above 100K". *Physica C*, **469**:2012–2014, 2009.

[9] Hussein. A. A and Hasan. N. A. "Study of the properties of YBCO superconductor compound in various preparation methods: A short review". *J. Appl. Sci. Nanotechnol.*, **3**(1):65–79, 2023.

[10] Abood. M. B and Al-Shakarchi. E. K. "Preparing of Superconductor Compound by Chemical Method". *Ph.D. thesis, Dept. Phys., Nahrain University*, 2025.

[11] Elmasli. S and Abdi. S. S. "Investigation of structural and superconducting properties of $YBa_2Cu_3O_{7-\delta}$ ceramics prepared by different sintering temperatures". *Journal of Superconductivity and Novel Magnetism*, **35**:363–371, 2022.

[12] Mohd Yusuf. N. N, Awang Kechik. M. M, Baqiah. H, SooKien. C, KeanPah. L, Shaari. A. H, and et al. "Structural and superconducting properties of thermal treatment-synthesised bulk $YBa_2Cu_3O_{7-\delta}$ superconductor: Effect of addition of SnO_2 nanoparticles". *Materials*, **12**(1):92, 2019.

[13] Abdulrahman. M. W and Hussain. F. I. "Synthesis of $Y_3Ba_5Cu_8O_{18-\delta}$ superconductor by auto-combustion reaction". *AIP Conf. Proc.*, **2123**:020085–1–020085–11, 2019.

[14] Güler. R. A, Varilci. A, and Toprak. M. "Structural and microstructural characterization of $YBa_2Cu_3O_{7-\delta}$ bulk samples synthesized using different methods". *Ceramics International*, **48**(9):12231–12238, 2022.

[15] Ghahramani. S, Shams. G, and Soltani. Z. "Comparative investigation of the effect of titanium oxide nanoparticles on some superconducting parameters of $Y_3Ba_5Cu_8O_{18\pm\delta}$ and $YBa_2Cu_3O_{7-\delta}$ composites". *Journal of Electronic Materials*, **50**(8):4727–4740, 2021.

[16] Arais. A. A, Shams. M. S, and Elbehiry. E. "The effect of Ni-Zn ferrite doping on the superconductivity of $Y_3Ba_5Cu_8O_{18}$ nanocomposite materials". *AIP Advances*, **10**:115012–1–115012–8, 2020.

[17] Slimani. Y, Hannachi. E, Hamrita. A, Ben Salem. M. K, Ben Azzouz. F, Manikandan. A, and Ben Salem. M. "Comparative investigation of the ball milling role against hand grinding on microstructure, transport and pinning properties of $Y_3Ba_5Cu_8O_{18\pm\delta}$ and $YBa_2Cu_3O_{7-\delta}$". *Ceramics International*, **44**(16):19950–19957, 2018.

[18] Larkin. P. J. "Infrared and Raman Spectroscopy: Principles and Spectral Interpretation". *Elsevier*, 2017.

[19] Al-Wabel. M, Elfaki. J, Usman. A, Hussain. Q, and Ok. Y. S. "Performance of dry water and porous carbon-based sorbents for carbon dioxide capture". *Environmental Research*, **174**:69–79, 2019.

[20] Pasieczna-Patkowska. S, Cichy. M, and Flieger. J. "Application of Fourier Transform Infrared (FTIR) Spectroscopy in Characterization of Green Synthesized Nanoparticles". *Molecules*, **30**(3):684, 2025.

[21] Scaria. S. S and Joseph. K. S. "Exploring the photocatalytic and cytotoxic potential of Quassia indica-derived bimetallic silver-zinc oxide nanocomposites". *Waste and Biomass Valorization*, **15**(11): 6251–6265, 2024.

[22] Chen. J, Ma. J, Fan. Q, Zhang. W, and Guo. R. "A sustainable chrome-free tanning approach based on Zr-MOFs functionalized with different metals through post-synthetic modification". *Chem. Eng. J.*, **474**:145453, 2023.

[23] Zhao. W, Huang. X, Zhang. Z, Chen. S, Du. M, Duan. D, and Cui. T. "Superconducting ternary hydrides: Progress and challenges". *Natl. Sci. Rev.*, **11**(7), 2024.

[24] Shoushtari. M. Z, Heidarzadeh. Gh, and Ghahfarokhi. S. M. "An investigation of $Y_3Ba_5Cu_8O_{18}$ doping with Ag nanoparticles and its application as superconductor". *Journal of Superconductivity and Novel Magnetism*, **31**:3475–3483, 2018.